

A step-by-step analytical procedure to estimate the in-situ stress state from borehole data

Original

A step-by-step analytical procedure to estimate the in-situ stress state from borehole data / Scelsi, G.; De Bellis, M. L.; Pandolfi, A.; Musso, G.; Della Vecchia, G.. - In: JOURNAL OF PETROLEUM SCIENCE AND ENGINEERING. - ISSN 0920-4105. - STAMPA. - 176:(2019), pp. 994-1007. [10.1016/j.petrol.2019.01.100]

Availability:

This version is available at: 11583/2725542 since: 2019-02-28T14:39:28Z

Publisher:

Elsevier

Published

DOI:10.1016/j.petrol.2019.01.100

Terms of use:

This article is made available under terms and conditions as specified in the corresponding bibliographic description in the repository

Publisher copyright

(Article begins on next page)

A step-by-step analytical procedure to estimate the in-situ stress state from borehole data

G. Scelsi · M.L. De Bellis · A. Pandolfi ·
G. Musso · G. Della Vecchia

Received: date / Accepted: date

Abstract Knowledge of in situ stress state of rock mass is fundamental for engineering, geological and geophysical applications. In situ stress state determination requires in principle the evaluation of the three principal stresses and the related principal direction, but it is widely recognized in the literature that the maximum horizontal stress is the most difficult component to accurately estimate. In the context of borehole methods, this paper proposes a step-by-step analytical procedure to estimate some bounds to the maximum horizontal stress starting from a geomechanical description of the rock and relying on information generally available in the engineering practice. The procedure is divided in substeps, each one requiring more information about the mechanical properties of the rock and on the geometrical properties of the failed portion of rock: more information available implies a lower uncertainty

Giulia Scelsi
Department of Civil and Environmental Engineering
Politecnico di Milano, Milano, Italy
E-mail: giulia.scelsi@polimi.it

Gabriele Della Vecchia
Department of Civil and Environmental Engineering
Politecnico di Milano, Milano, Italy
E-mail: gabriele.dellavecchia@polimi.it

Anna Pandolfi
Department of Civil and Environmental Engineering
Politecnico di Milano, Milano, Italy
E-mail: anna.pandolfi@polimi.it

Guido Musso
Department of Structural, Geotechnical and Building Engineering
Politecnico di Torino, Torino, Italy
E-mail: guido.musso@polito.it

Maria Laura De Bellis
Department of Innovation
Università del Salento
E-mail: maria.laura.debellis@unisalento.it

on in situ stress estimate. Furthermore the procedure is analytical, i.e. just a spreadsheet is needed for its implementation. Finally, just information easy to determine and generally available in the context of reservoir engineering is required. The aim of the work is thus to provide a rigorous but simple analytical tool that can be used in engineering practice to estimate some bounds to the maximum horizontal in situ stress state. The approach is finally validated by means of both numerical simulations performed with a sophisticated numerical tool and experimental field data coming from the literature.

Keywords In situ stress · breakout failure · borehole

1 Introduction

Knowledge of in situ stress state is fundamental for the solution of many problems not only in the field of civil, mining and petroleum engineering, but also for geological and geophysical applications. For instance, stress concentration around underground openings is significantly affected by the in situ original stress state, and its knowledge is mandatory for any deformation and instability evaluation of tunnels and shafts. When dealing with oil and gas applications (e.g. borehole excavations, sand production management and stimulation interventions), the knowledge of the stress state and its variation is required before and during reservoir depletion, as well as to predict the distribution and the propagation of cracks as a consequence of fracking jobs.

In situ stress state evaluation implies the determination of six independent quantities, namely the six independent components of the Cauchy second order tensor with respect to a given coordinate system. However, it is most common in engineering practice to determine the three principal stresses and to identify the related principal directions. The initial stress state of horizontal and homogeneous soil layers, which are commonly originated by deposition, is generally evaluated by assuming that the vertical and the horizontal directions are principal ones: the vertical stress is considered coincident with the overburden, while the horizontal one is evaluated by means of the K_0 concept (Jaky, 1944, Schmidt, 1966). When the geometric configuration is more complex, numerical simulations of the deposition process are usually performed by increasing the unit weight of the material. When dealing with rock formations, the problem of identifying the initial stress state is much more complicated, being the result of many processes and mechanisms, involving tectonic, gravity and residual stresses. At a smaller scale, the in situ state of stress is also locally influenced by the presence of cavities and discontinuities. Uncertainties related to the exact geological history, the constitutive laws and the detailed structure of the rock mass imply that no numerical computations can be performed to reliably simulate the whole geological history and thus to estimate the in situ stress field (Zang and Stephansson, 2010). It is in fact widely accepted that stresses in the rock can only be inferred by disturbing the rock and evaluating

the induced mechanical consequences, that depend on the original stress itself.

According to Amadei and Stephansson (1970), classical crustal in-situ measurement techniques require either a well bore (e.g. breakout analysis, hydrofrac) or core materials (e.g. overcoring, strain relief). Despite coring methods are widely used techniques in the engineering application of stress measurement, they suffer of some limitations related to the maximum depth allowed and to the small volume involved in the measurement. Borehole methods applicability is vice versa limited just by the maximum borehole depth. Zoback et al (2003) evidenced the advantages and the reliability of borehole methods to determine stress orientation and magnitude in deep wells, highlighting the role of a sound geomechanical model of the subsurface and of wellbore imaging devices, like ultrasonic televiewers and electrical imaging tools, to yield detailed information about wellbore failure.

The classical strategy that is employed to characterize the stress field (see, e.g. Zoback et al, 2003 and Zoback, 2007) is based on the following steps: i) The vertical stress is determined from the equilibrium in the vertical direction, i.e. by integration of density logs; ii) The orientation of the principal stresses can be determined from wellbore observations, recent geologic observations and earthquake focal mechanisms; iii) The minimum principal stress can be estimated from the analysis of hydraulic fracturing and leak-off tests (see, e.g. Zoback and Healy (1992) and Haimson et al (2009)); iv) Pore pressure can be either measured directly or estimated with some caution from geophysical logs or seismic data. Generally the vertical stress is assumed to be a principal one, so that the remaining two directions are supposed to be horizontal. This assumption is reliable for non-active regions or regions already relaxed from previous tectonical stress. In fact, according to Bell (2003), the free surfaces of sedimentary basins are generally horizontal, so that the principal stress directions are in good approximation vertical and horizontal. Accordingly, it is recognized by the relevant literature that the maximum horizontal principal stress is the most difficult component to accurately estimate. Some bounds to the maximum horizontal stress can be provided by the application of the Anderson faulting theory together with Mohr-Coulomb failure. For any given depth of a rock mass, some maximum values of the difference between the maximum and the minimum principal stresses can be argued, relying on the assumption that the stresses in the earth crust cannot exceed the frictional strength of pre-existing faults. Of course, this argument is valid at a broad scale and, locally, exceptions can exist. Furthermore, an estimate of fault friction angle is needed. Applications are shown in Moos and Zoback (1990), Wiprut and Zoback (2000) and Zoback et al (2003). Other boundaries to the maximum horizontal principal stress are provided by compressive failure data recovered on circular borehole walls as a consequence of excavation and pressurization by means of drilling muds. Such bounds can be determined from limitations imposed by the shear resistance of the material. In fact, when a well or a borehole is drilled, the stresses that were previously supported by the exhumed material

are transferred to the region surrounding the well. The resultant stress concentration, well understood in terms of elastic theory, amplifies the difference between the virgin (far-field) principal stresses. The so-called *breakout* failures are related to a shear failure process that occurs when the maximum hoop stress around the hole increases to such an extent that the shear resistance of the rock is exceeded. In the case of vertical wellbore and vertical principal stress, the azimuth of the breakout failures is coincident with the direction of the minimum horizontal principal stress. The possibility of multiple determination of stress in an individual well, and the ability to check for regional consistency among numerous wells, make breakout data valuable indicators of in situ stress state. Breakout failures have been exploited to determine some limiting values of the maximum horizontal principal stress in Leeman (1964), Bell and Gough (1979), Zoback et al (1986). A relevant role in breakout failure analysis is provided by the failure criterion used to describe rock behaviour: Moos and Zoback (1990) provided solutions by considering a Galileo-Rankine criterion for the compressive strength of the rock, characterized by a constant value, while Vernik and Zoback (1992) provided estimates via the Weibols and Cook (1968) strain energy failure criterion. Zoback et al (1985) exploited the elastic Kirsch solution and Mohr-Coulomb failure criterion to highlight the role of breakout shape and inelastic deformation around the borehole, as later evidenced by Barton et al (1988), Aadnoy et al (2013) and Della Vecchia et al (2014). Drilling induced tensile fractures are another failure mechanism which could give significant information about the entity and the direction of the horizontal maximum principal stress. These fractures form on the wall of the borehole with an azimuth coincident with the direction of the maximum horizontal stress, when a principal stress is locally tensile.

According to this picture, it is evident that the estimate of in situ rock stress state for engineering purposes suffers, as any other geomechanical application, of a relevant problem: due to the complex stress-strain behavior of rocks, sophisticated theoretical and numerical tools are in principle needed to obtain reliable predictions. The applicability of such models is however limited by the effort needed in their calibration and in their numerical implementation, which is generally unaffordable for common engineering applications. In order to overcome this seeming insurmountable dichotomy between reliable predictions and applicability for engineering purposes, this paper presents a step-by-step analytical procedure to estimate the in situ maximum horizontal stress exploiting borehole failure data. The procedure is divided in substeps, each substep implying an increasing degree of detail about the knowledge of the mechanical properties of the materials involved and on the geometrical properties of the failed portions of rocks. Of course, the higher the quantity of information available, the lower the uncertainty on the estimated stress. It is worth underlying that the procedure is purely analytical: it is thought to be implemented in a simple spreadsheet and no programming or dedicated software are required. Moreover, all the parameters required are easy to determine: in the proposed version of the procedure the rock will be characterized

in terms of uniaxial strength and friction angle, while the only information needed from the field is the orientation of the faults (if any) and the size of the breakout failure (if any). The procedure has been successfully validated basing on both numerical analyses and case histories from the literature. Numerical analysis has been performed by means of a Finite Element approach, capable of simulating the mechanical behaviour of the rock surrounding the borehole by means of a brittle damage constitutive model for geological media recently proposed in De Bellis et al (2016, 2017). The model in fact proved able to simulate the mechanical behaviour of both sedimentary and crystalline rocks, both in the pre- and the post-peak stages, showing to be particularly suitable for materials showing a brittle behavior. The approximation provided by the simplified analytical solution to the results obtained by means of such a sophisticated numerical tool is excellent, at least for breakout opening lower than 90° . Appreciable agreement has been also obtained by applying the procedure to in situ experimental data presented in the literature.

2 Steps involved in the procedure: methodology

The procedure to estimate the maximum horizontal stress detailed below involves four substeps: Step 1 is based on Anderson faulting theory, and just a broad estimate of the friction angle of the faults is required. Step 2 is based on the application of the Kirsch elastic solution for the redistribution of stresses around a borehole in plane strain conditions: depending on the azimuth and the far-field stress state, the maximum and minimum principal stress on borehole wall coincides with different stress components, i.e. radial, hoop or vertical. Stress distribution around the hole according to the Kirsch solution, together with simple visual information obtained along borehole depth about the orientation of drilling-induced failure, allows a refinement of the bounds of the far field stress obtained in Step 1. It is worth noting that Step 2 does not require any information about strength properties of the material at the borehole scale. Step 3 takes advantage on both the information about the presence of tensile and breakout failures on borehole wall and the knowledge of rock failure criterion, further reducing the bounds identified in Step 2. Finally, if also the size of the borehole breakout is known, Step 4 will provide a unique value of the maximum horizontal stress.

In the following, S_v represents the total principal vertical virgin stress, S_H the total maximum horizontal virgin stress and S_h the total minimum horizontal virgin stress. According to the Introduction, S_v and S_h are assumed to be known in term of both magnitude and direction. When dealing with the mechanical behaviour of rocks, the stress to be used in the failure criteria are effective stress, indicated as S'_v , S'_h and S'_H for the vertical and the two horizontal stress directions, respectively. The effective stress tensor, in general indicated as σ'_{ij} is evaluated according to Biot as

$$\sigma'_{ij} = \sigma_{ij} - \alpha p_w \delta_{ij} \quad (1)$$

where σ_{ij} is the total Cauchy stress tensor, p_w is the pore fluid pressure, α the Biot coefficient and δ_{ij} is the Kronecker delta. In the following, $\alpha = 1$ is assumed and the rock is always considered as saturated.

2.1 Step 1: limits on the stress state from the tectonic regime

The idea of using the Anderson (1951) faulting theory to estimate some broad limits on the in situ stress state relies on the assumption that the phenomena of brittle fracture studied at the laboratory scale appear to be reproduced in nature by geological structures (Zang and Stephansson, 2010): faults thus result from brittle failure, according to the Mohr-Coulomb failure criterion. According to Anderson, tectonic stress near the Earth crust can be classified into normal, strike-slip and reverse, depending on the relative combination of the principal stresses (Table ??). At each depth, the Anderson faulting theory

Regime	S_1	S_2	S_3
Normal NF	S_v	S_H	S_h
Strike-slip SS	S_H	S_v	S_h
Reverse RF	S_H	S_h	S_v

Table 1 Principal stresses in the different tectonic regimes

defines some relations between the values of stresses, according to the strength criterion of the material. Let us assume that the Mohr-Coulomb criterion holds in the form

$$\sigma'_1 = C + N_\phi \sigma'_3 \quad (2)$$

being σ'_1 and σ'_3 the maximum and minimum principal effective stress, respectively, C the uniaxial compressive strength and N_ϕ a function of the friction angle ϕ' , i.e. $N_\phi = (1 + \sin \phi') / (1 - \sin \phi')$.

For any tectonic regime, a relation between some of the in situ principal stresses can be identified, corresponding to the fulfilment of Equation 1:

- Normal fault (NF) $S'_v > S'_H > S'_h$

$$\frac{\sigma'_1}{\sigma'_3} = \frac{S'_v}{S'_h} = \frac{C}{S'_h} + N_\phi \quad (3)$$

- Strike-slip fault (SS) $S'_H > S'_v > S'_h$

$$\frac{\sigma'_1}{\sigma'_3} = \frac{S'_H}{S'_h} = \frac{C}{S'_h} + N_\phi \quad (4)$$

- Reverse fault (RF) $S'_H > S'_h > S'_v$

$$\frac{\sigma'_1}{\sigma'_3} = \frac{S'_H}{S'_v} = \frac{C}{S'_v} + N_\phi \quad (5)$$

For a given depth (and thus a given overburden stress) and pore pressure, the equations above identify a region in the horizontal stresses plane: the in situ stress state of the material, that cannot support a shear stress greater than the one identified by the failure criterion, must lay inside or on the boundaries of the region. Detailed information about this procedure can be found in Zoback et al. [?] and Moos and Zoback [?].

This first step of the procedure needs just a broad estimate of the strength parameters of the material involved: as it has been shown from laboratory studies on a large variety of rock samples and from in situ experiments in different fault regimes, the friction coefficient generally ranges from 0.6 to 1.0 (i.e. ϕ' between 30° and 45°). Being not known a priori if the major role in terms of failure is provided by the faults or by the core material, in this case just literature data of friction angle for the studied lithotypes can be used. As for the value of the uniaxial strength, it is worth evidencing that in petroleum engineering applications the role of C in drawing stress polygons is generally neglected.

In the following, each step of the procedure is applied to a well documented case study from the literature, i.e. a 2-km-deep research borehole (Hole-B) drilled in the context of the drilling project investigating the Chelungpu Fault (Taiwan). Information about material properties and in situ stress state can be found in different studies present in the literature (e.g. Wu et al., 2007, Hung et al., 2007, Lin et al., 2009, Haimson et al., 2009); leak-off tests allowed the determination of the variation of the minimum horizontal principal stress S_h with depth, while from the interpretation of *formation microscanner* FMS results breakout widths have been estimated for depths between 940 m and 1310 m. Figure ?? shows the stress state limits that can be identified for a depth of 1000 m, where the rock mass is characterized by a far-field minimum horizontal principal stress equal to $S'_h = 10.8$ MPa and a far-field vertical effective stress $S'_v = 14.7$ MPa: S'_H is limited by a lower bound $S'_H = S'_h = 10.8$ MPa and by an upper bound $S'_H = 39.8$ MPa, corresponding to a stress anisotropy $S'_H/S'_h = 3.7$ deriving from the limit corresponding to the strike-slip regime. Values of $\phi' = 35^\circ$ and saturated density $\rho_{sat} = 2.5$ g/cm³ have been used, according to Haimson & Rudnicki (2009) and Wang (2011). Pore pressure has been assumed to be hydrostatic.

2.2 Step 2: limits on the stress state from failure orientation

The estimate of the bounds on the value of the maximum horizontal stress identified at Step 1 can be refined by means of a visual inspection of borehole failure, performed, e.g., by ultrasonic televiewers. It is well known that, in the case of isotropic linear elastic behaviour, the perturbation to the stress field induced by a circular hole can be calculated with analytical solutions. In this case, the axi-symmetric problem of a circular hole (having an internal radius a and subjected to a uniform internal pressure p_i) in a linear elastic infinite rock mass is considered. The radial coordinate r , i.e. the distance from borehole

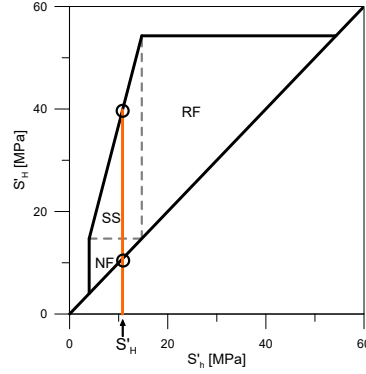


Fig. 1 Admissible stress polygon and limits from tectonic regimes for the Chelungpu fault site.

center, ranges between a and ∞ . The angle θ , positive counterclockwise, is defined as the angle between the radius considered and the direction of the maximum horizontal stress (see figure ??). The net pressure p_{net} is defined as the difference between p_i and the pressure of the pore fluid, p_w : $p_{\text{net}} = p_i - p_w$. Under the assumption of plane strain, the solution for the perturbation of the stress field due to the hole has been proposed by Kirsch (see, e.g. Jaeger [?]), as a function of the maximum and the minimum horizontal effective far-field stresses, S'_H and S'_h . In terms of effective radial, hoop and shear stress, the Kirsch solution reads:

$$\begin{aligned}\sigma'_r &= \frac{1}{2}(S'_H + S'_h) \left[1 - \left(\frac{a}{r}\right)^2 \right] + p_{\text{net}} \left(\frac{a}{r}\right)^2 + \frac{1}{2}(S'_H - S'_h) \left[1 - 4\left(\frac{a}{r}\right)^2 + 3\left(\frac{a}{r}\right)^4 \right] \cos 2\theta, \\ \sigma'_\theta &= \frac{1}{2}(S'_H + S'_h) \left[1 + \left(\frac{a}{r}\right)^2 \right] - p_{\text{net}} \left(\frac{a}{r}\right)^2 - \frac{1}{2}(S'_H - S'_h) \left[1 + 3\left(\frac{a}{r}\right)^4 \right] \cos 2\theta, \\ \tau_{r\theta} &= -\frac{1}{2}(S'_H - S'_h) \left[1 + 2\left(\frac{a}{r}\right)^2 - 3\left(\frac{a}{r}\right)^4 \right] \sin 2\theta,\end{aligned}\tag{6}$$

where σ'_θ , σ'_r and $\tau_{r\theta}$ are the effective hoop, radial and shear stress, respectively.

Under the assumption of drilling operations performed in plane strain conditions in the vertical direction, the principal stresses on borehole wall ($r = a$) and $\theta = 0$ can be expressed, according to the Kirsch solution, as

$$\begin{aligned}\sigma'_r &= p_{\text{net}} \\ \sigma'_\theta &= 3S'_h - S'_H - p_{\text{net}}, \\ \sigma'_z &= S'_v + \Delta\sigma'_z = S'_v + 2\nu(S'_h - S'_H).\end{aligned}\tag{7}$$

The increment $\Delta\sigma'_z$ due to borehole excavation has been evaluated by assuming null vertical strain increment ($\Delta\varepsilon_z = 0$) during the drilling and mud pressur-

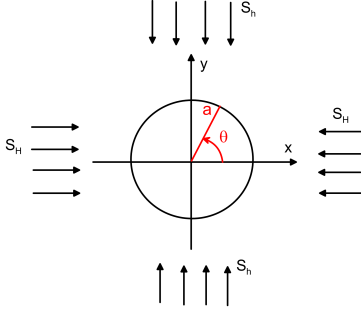


Fig. 2 Radial coordinates for the circular hole

ization processes, coherently with the elastic solution introduced. The increments of radial and hoop stress in this case are calculated as $\Delta\sigma'_r = p_{net} - S'_h$ and $\Delta\sigma'_\theta = \sigma'_\theta - S'_H = 2'S_H - S'_h - p_{net}$, so that $\Delta\sigma'_z = 2\nu(S'_H - S'_h)$ (being ν the Poisson coefficient of the rock).

If the stress components are divided by the minimum effective far-field horizontal stress S'_h , the role of the far-field stress anisotropy S'_H/S'_h is highlighted:

$$\begin{aligned} \frac{\sigma'_r}{S'_h} &= \frac{p_{net}}{S'_h} \\ \frac{\sigma'_\theta}{S'_h} &= 3 - \frac{S'_H}{S'_h} - \frac{p_{net}}{S'_h} \\ \frac{\sigma'_z}{S'_h} &= \frac{S'_v}{S'_h} + 2\nu \left(1 - \frac{S'_H}{S'_h} \right). \end{aligned} \quad (8)$$

Equation (??) represents three lines in the σ'/S'_h vs. S'_H/S'_h plane, that can be easily drawn when the relevant information about S'_v , S'_h and p_{net} are known: for example, plotting the three lines allows the visualization of the maximum, the intermediate and the minimum principal stresses on borehole wall for $\theta = 0$, i.e. when tensile failure is anticipated.

Figure ?? shows an example of the evolution of the stress state in $\theta = 0$ as a function of the horizontal anisotropy ratio for $S'_v = 14.7$ MPa and $p_{net} = 0$ MPa. The maximum stress anisotropy considered in the example is the one identified in Step 1, i.e. $S'_H/S'_h \leq 3.7$ (see section ??). It is evident that for low values of S'_H/S'_h , the minimum principal stress is the radial one, while for high values of S'_H/S'_h the hoop stress becomes the minimum one. If a visual information about tensile failure is provided, it is possible to determine what is the direction of the minimum principal stress: vertical fractures are generally obtained if the hoop stress is minimum, horizontal fractures if the vertical stress is minimum, concentric fractures if the radial stress is minimum (see, e.g Zang and Stefansson, 2010). Once the minimum principal stress is identified, the relevant zone according to Equation (??) can be identified, and thus a further limitation in stress anisotropy is obtained. According to the example, in the

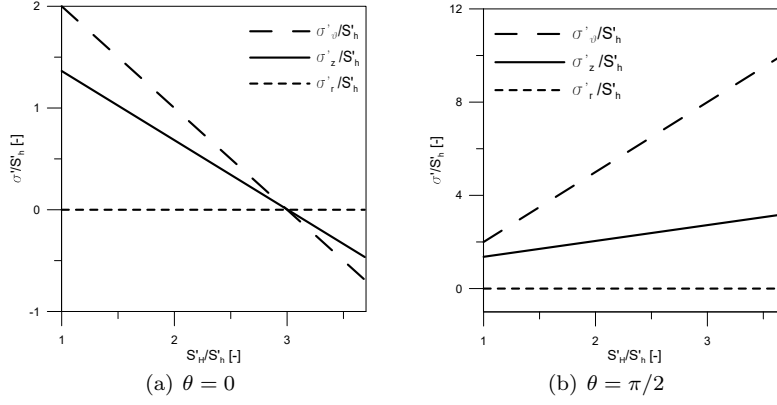


Fig. 3 Relation between normalized principal components as a function of horizontal stress anisotropy S'_H/S'_h ($S'_v = 14.7$ MPa, $\nu = 0.34$, $p_{net} = 0$).

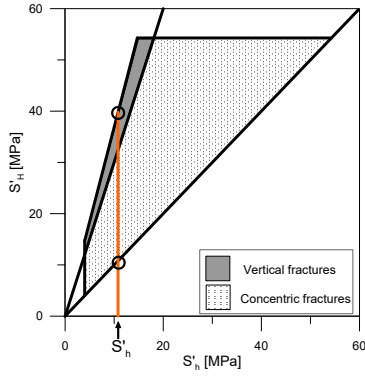


Fig. 4 Identification of the regions where the different tensile failure orientations can potentially take place.

presence of vertical fractures σ'_θ has to be the minimum principal stress, and so $3 \leq S'_H/S'_h \leq 3.7$; if concentric fractures are detected, σ'_r is the minimum principal stress, so that $1 \leq S'_H/S'_h \leq 3$. The limiting anisotropies separating the different tensile failure orientation can be plotted in the stress polygon, as shown in Figure ??, where the line $S'_H = 3 \cdot S'_h$ divides vertical and concentric fractures.

The same logical path can be applied on the borehole wall in $\theta = \pi/2$, when shear failure is anticipated: also in this case the fault pattern is dependent on which components are the maximum and the minimum ones. In this case the principal effective stresses on borehole wall ($r = a$) reads:

$$\begin{aligned} \sigma'_r &= p_{net} \\ \sigma'_\theta &= 3S'_H - S'_h - p_{net} \\ \sigma'_z &= S'_v + 2\nu(S'_H - S'_h), \end{aligned} \quad (9)$$

and in non dimensional form

$$\begin{aligned}\frac{\sigma'_r}{S'_h} &= \frac{p_{net}}{S'_h} \\ \frac{\sigma'_\theta}{S'_h} &= 3\frac{S'_H}{S'_h} - 1 - \frac{p_{net}}{S'_h} \\ \frac{\sigma'_z}{S'_h} &= \frac{S'_v}{S'_h} + 2\nu \left(\frac{S'_H}{S'_h} - 1 \right).\end{aligned}\tag{10}$$

Figure ?? shows the evolution of the stress components in $\theta = \pi/2$ as a function of the horizontal anisotropy ratio and it clearly illustrates that in this specific case for all the admissible anisotropy ratios the radial effective stress is always the minimum principal stress and the hoops stress is always the maximum principal stress ($\sigma'_r < \sigma'_z < \sigma'_\theta$). In this specific case, such an information cannot provide any further refinement of S'_H bounds, because just a type of breakout failure is predicted. If viceversa also the lines predicted by (??) would cross themselves, then the same logic of Figure ?? can be followed: depending on fault orientation in the breakout zone, the relevant region in term of stress anisotropy could be identified.

2.3 Step 3: limits on the stress state from rock failure criterion

According to equation ??, under the assumption of plane strain conditions during drilling operations, the complete effective state of stress can be written on borehole wall ($r = a$), allowing to determine, once the strength parameters of the materials are known, if failure conditions are met. According to the literature, the evolution of the effective hoop stress on the borehole wall can be considered as a proxy to determine which zones of the borehole can be subjected to shear failure and which ones to tensile failures. Writing σ'_θ as a function of θ in $r = a$ leads to the expression

$$\sigma'_\theta(a, \theta) = (S'_H + S'_h) - p_{net} - 2(S'_H - S'_h) \cos 2\theta,\tag{11}$$

that shows that the minimum value $3S'_h - S'_H - p_{net}$ is achieved for $\theta = 0$ or $\theta = \pi$, while the maximum one, $3S'_H - S'_h - p_{net}$, for $\theta = \pi/2$, or $\theta = 3/2\pi$.

If the value of S_v , S_h , p_{net} and p_w are known from previous determinations, as well as the elastic parameters and the failure properties of the material, certain boundaries for S_H can be obtained basing on the occurrence of compression or tensile failure on the borehole wall.

2.3.1 Maximum horizontal stress S_H from breakout failure

If a breakout failure occurs, a first broad estimate of a lower boundary for the maximum horizontal stress S_H^{\min} can be obtained assuming that failure just started, involving a single point on the borehole wall rather than a wider volume of rock. It is known that breakout failure will generally start at $\theta = \pi/2$,

where σ'_θ coincides with the local maximum principal stress. Expressing the principal stresses as a function of the far-field virgin stresses, it follows that for $\theta = \pi/2$, equation (??) holds.

Once expressed the values of the principal effective stresses σ'_θ , σ'_r and σ'_z as a function of the only unknown S'_H , the problem to be solved reduces to finding S'_H such that

$$f_C(\sigma'_z(S'_H), \sigma'_r, \sigma'_\theta(S'_H)) = f_C(S'_H) = 0, \quad (12)$$

where $f_C(\sigma'_{ij}) = 0$ is a suitable shear failure criterion of the material. The methodology is intended to work for any failure criterion, and analytical solutions can be found for the Mohr-Coulomb, Hoek-Brown and Mogi-Coulomb failure criteria, just to cite a few (Scelsi, 2017). For the sake of simplicity, in the following part just the Mohr-Coulomb (MC) criterion will be considered, being its parameters the easiest to determine.

The Mohr-Coulomb failure criterion in terms of maximum and minimum principal stresses (σ'_1 and σ'_3 respectively) reads:

$$\sigma'_1 = C + N_\phi \sigma'_3. \quad (13)$$

where C is the uniaxial compression strength and $N_\phi = \frac{1 + \sin \phi'}{1 - \sin \phi'}$, being ϕ' the internal friction angle. For $\theta = \pi/2$, where breakout failure are anticipated, the maximum principal stress is generally σ'_θ , while the minimum principal stress is not known a priori. From the analytical point of view, two cases should be considered:

- If the minimum principal stress is σ'_r , the value of S'_H corresponding to failure (for given S'_v and S'_h) is

$$S'_H{}^{MC} = \frac{1}{3} [S'_h + (1 + N_\phi)p_{\text{net}} + C] \quad \text{if } \sigma'_3 = \sigma'_r, \quad (14)$$

- If the minimum principal stress is σ'_z , it follows that

$$S'_H{}^{MC} = \frac{C + N_\phi S'_v + S'_h(1 - 2\nu N_\phi) + p_{\text{net}}}{3 - 2\nu N_\phi} \quad \text{if } \sigma'_3 = \sigma'_z. \quad (15)$$

In the case that breakout failure occurs, $S'_H{}^{MC}$ has to be considered as a lower bound for S'_H , i.e. in order to have failure, a value of $S'_H \geq S'_H{}^{MC}$ is needed. Viceversa, if breakout failure does not occur, then $S'_H{}^{MC}$ has to be considered an upper bound for S'_H .

Figure ?? shows the line expressed by equation ?? taking $C = 79.5$ MPa and $\phi' = 35^\circ$, representing a bound for the maximum horizontal stress S'_H , thus identifying two possible domains for S'_H according to the detection of breakout failures. Due to the presence of shear failures in the considered borehole section, it can be stated that S'_H has to be greater than $S'_H > 30.1$ MPa (therefore $S'_H/S'_h > 2.8$) for the specified S'_h value. Step 3 of the procedure, accounting for breakout failure, is shown in Figure ??: the admissible stress state has to fall between the limits deriving from Anderson faulting theory (Step 1) and from the detection of breakout.

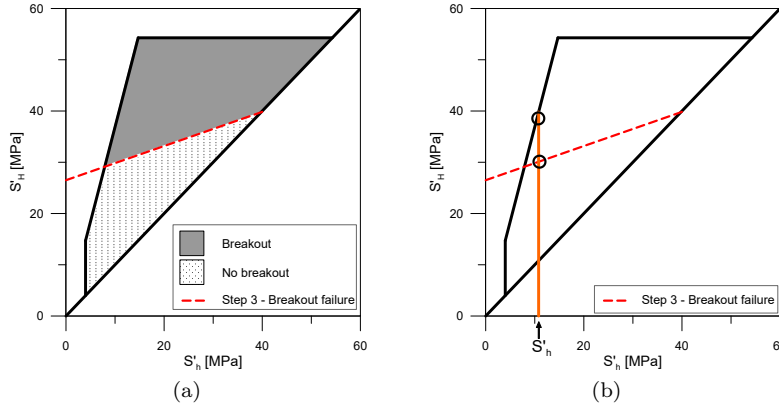


Fig. 5 Stress polygon with the dashed red line identifying the lower bounds for S'_H in order to have breakout failures according to the Mohr-Coulomb failure criterion.

2.3.2 Maximum horizontal stress S_H from tensile failure

If a tensile failure occurs, a first broad estimate of a lower boundary for the maximum horizontal stress S'_H can be obtained assuming that failure just started, involving a single point on the borehole wall rather than a wider volume of rock. It is known that drilling induced tensile failure will generally start at $\theta = 0$, where σ'_θ coincides with the local minimum principal stress. Expressing the principal stresses as a function of the far-field virgin stresses, it follows that for $\theta = 0$, equation (??) holds.

Once expressed the values of the principal effective stresses σ'_θ , σ'_r and σ'_z as a function of the only unknown S'_H , the problem to be solved reduces to finding S'_H such that

$$f_T(\sigma'_z(S'_H), \sigma'_r, \sigma'_\theta(S'_H)) = f_T(S'_H) = 0, \quad (16)$$

where $f_T(\sigma'_{ij}) = 0$ is a suitable tensile failure criterion of the material. Also in this case, the methodology is intended to work for any failure criterion. For the sake of simplicity, in the following part just the Galileo-Rankine (G) criterion will be considered, because it requires just one parameter to determine, i.e. the tensile strength S_T .

The Galileo failure criterion depends only on the minimum principal stress (σ'_3), so that

$$\sigma'_3 = S_T. \quad (17)$$

For $\theta = 0$, where tensile failures are anticipated, the minimum principal stress is σ'_θ . The value of S'_H corresponding to failure (for given S'_h) is

$$S'^G_H = 3S'_h - S_T - p_{net}. \quad (18)$$

In the case that tensile failure occurs, S'^G_H has to be considered as a lower bound for S'_H , i.e. in order to have failure, a value of $S'_H \geq S'^G_H$ is needed.

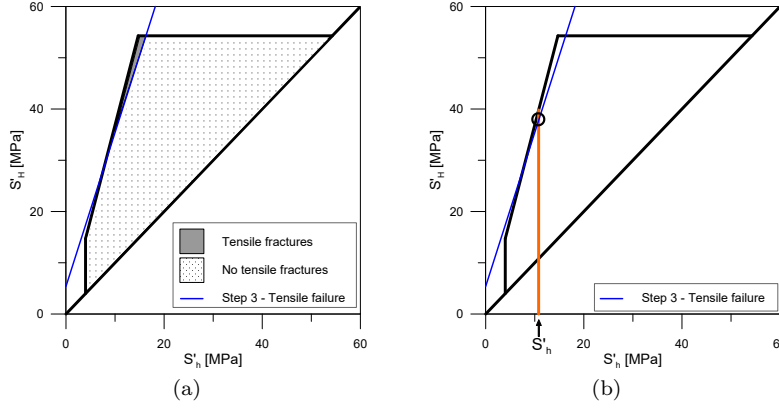


Fig. 6 Stress polygon with the blue dashed line identifying the lower bounds for S'_H in order to have tensile failures according to the Galileo strength criterion.

Viceversa, if tensile failure does not occur, then S'^G_H has to be considered an upper bound for S'_H .

Figure ?? shows the line expressed by equation ??, representing an upper bound for the maximum horizontal stress S'_H , since no tensile fractures have been registered in the section taken as example. Two possible domains for S'_H are identified according to the detection of tensile failures. A value $S_T = 5.4$ MPa, as reported by Haimson & Rudnicki (2009), has been considered. Combining this information with that derived in ??, it can be stated that S'_H ranges between 30.1 MPa (Fig. ??) and 37.8 MPa (corresponding to $2.8 < S'_H/S'_h < 3.5$) for the specified S'_h value.

2.4 Step 4: accounting for breakout size

In order to further reduce the uncertainties related to the determination of S'_H , an analytical solution was provided in Della Vecchia et al (2014), taking into account also the information about the size of breakout failures. Step 4 thus not only need the knowledge of the parameters characterizing the rock failure criterion, but also detailed outputs from dipmeters or borehole televiewers during breakout logging in vertical boreholes. According to Barton et al. (1998), an angle α_b that subtends the breakout zone from the center of the hole can be introduced, as well as the angle θ_b ($\theta_b = \pi/2 - \alpha_b/2$), positive clockwise, between the direction of the maximum horizontal principal stress and the radius passing from the extremity of the breakout zone. The proposal of Della Vecchia et al (2014) is based on the assumption that the size of the breakout measured in situ at the well scale coincides with the size of the yielding zone that would originate in the same conditions in an elastic perfectly plastic material. Accordingly, the principal effective stresses on borehole wall for $\theta = \theta_b$ can be expressed as

$$\begin{aligned}
\sigma'_\theta &= S'_H + S'_h - p_{\text{net}} - 2(S'_H - S'_h) \cos 2\theta_b, \\
\sigma'_z &= S'_v + \Delta\sigma'_z, \\
\sigma'_r &= p_{\text{net}}.
\end{aligned} \tag{19}$$

The increment $\Delta\sigma'_z$ due to borehole excavation has been calculated, also in this case, assuming plane strain ($\Delta\varepsilon_z = 0$). Assuming that for $\theta = \theta_b$ the material is prone to yield, the vertical stress can be evaluated using both the elastic solution, (??), and imposing that the stress satisfies the yielding condition ((??) if a Mohr-Coulomb yield surface is assumed). The solution obtained is a function both of the size of the yield locus and of the particular yield function chosen. As in the elastic case, the maximum compression hoop stress acts for $\theta = \pi/2$. Being σ'_θ the maximum stress, the minimum is not known a priori. If σ'_r is the minimum effective stress, then the maximum horizontal stress is

$$S'_H = \frac{C - S'_h(1 + 2 \cos 2\theta_b) + (1 + N_\phi)p_{\text{net}}}{1 - 2 \cos 2\theta_b}, \quad \sigma'_3 = \sigma'_r. \tag{20}$$

If the minimum stress is σ'_z , then:

$$S'_H = \frac{C + N_\phi S'_v + S'_h[-1 - 2 \cos 2\theta_b(1 - \nu N_\phi)] + p_{\text{net}}}{1 + 2 \cos 2\theta_b(\nu N_\phi - 1)}, \quad \sigma'_3 = \sigma'_z. \tag{21}$$

If the breakout size is known, a unique value of the maximum horizontal stress S_H can be determined. In the example, σ'_r is taken as the minimum principal stress, assuming the principal components in $\theta = \theta_b$ to have the same relations as those in $\theta = \pi/2$. Equation ??, plotted in Figure ??, identifies a single value of S'_H for each minimum horizontal stress S'_h : it is evident that the stress states with a known breakout width are greater than the stresses deriving only from breakout failure starting at $\theta = \pi/2$. For the S'_h value at 1000 m depth, equal to 10.8 MPa, the maximum horizontal stress S'_H takes the value of 34.8 MPa (corresponding to $S'_H/S'_h = 3.2$); this value falls between the limits obtained in Step 3.

Table ?? summarises the bounds for S'_H obtained using the proposed approach for the Chelungpu site at 1000 m. It is evident that the greater the detail of the analysis and the larger the information available, the lower the uncertainty of S'_H estimate.

3 Numerical validation of the procedure

The procedure proposed is characterized by a continuous refinement of the bounds in which the real value of S'_H should lie. If information on the mechanical properties of the material and the size of the breakout failures is available, then Step 4 allows the determination of a unique value of S'_H . As a consequence, a relevant issue is provided by the reliability of equations ?? and ?. In Della Vecchia et al. (2014), FEM simulations were performed to check if the

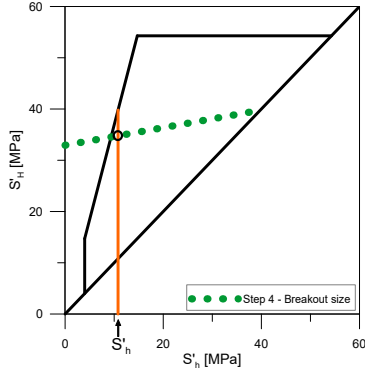


Fig. 7 Stress polygon with green dotted line identifying the value of S'_H at $\theta_b = 68^\circ$ (eq. ??).

Step	$S'_H{}^{min}$ [MPa]	$S'_H{}^{max}$ [MPa]	Information needed
1	10.8	39.8	Broad estimate of ϕ'
2	Data not available	Data not available	Visual information of failures
3	30.1	37.8	C, ϕ', S_T
4	34.8	34.8	$C, \phi', \text{breakout width}$

Table 2 Bounds for S'_H for each step using the proposed procedure for Chelungpu-Hole B at 1000 m

analytical equations proposed were consistent with the mechanical behaviour of an elastic-perfectly plastic material at the borehole scale. However, rocks hardly behave as perfectly plastic materials, often showing a brittle stress-strain response under stress paths that leads the material to failure: stress redistribution due to material failure and the consequent induced anisotropy cannot be accounted for when perfect plasticity is assumed. In order to validate step 4 of the procedure, the outcome of equations ?? and ?? has been compared with the results of numerical simulations performed by considering the complex stress-strain behaviour of the rock, including the possibility of brittle failure. In particular, borehole excavation has been simulated via the Finite Element Method, assuming the stress-strain relation to be described by the brittle-damage constitutive model presented in De Bellis et al (2016, 2017). The model is based on an explicit micromechanical construction of connected patterns of parallel equi-spaced faults, such that the rock undergoes compatible deformations and remains in static equilibrium down to the micromechanical level. In particular, given a single family of faults characterized by a spacing L and a unit normal \mathbf{N} to the plane of the faults, the deformation of the rock is evaluated as the sum of the deformation of the homogeneous porous matrix $\boldsymbol{\varepsilon}^m$ and the deformation due to fault opening $\boldsymbol{\varepsilon}^f$:

$$\boldsymbol{\varepsilon} = \boldsymbol{\varepsilon}^m + \boldsymbol{\varepsilon}^f = \boldsymbol{\varepsilon}^m + \frac{1}{2L}(\boldsymbol{\Delta} \otimes \mathbf{N} + \mathbf{N} \otimes \boldsymbol{\Delta}) \quad (22)$$

being Δ the displacement jump of the faults (i.e. the relative displacement of the two sides of the fault) and \otimes the dyadic product between two vectors.

A relevant feature of the model is that the fracture patterns are not arbitrary, but their inception, orientation and spacing follow from energetic consideration. The constitutive model is derived within a thermodynamic framework, assuming the existence of an incremental work of deformation which accounts for reversible and dissipative behaviours of the material. Formally, the fracture pattern and the effective stress at the representative elementary volume level at time t_{n+1} is obtained incrementally, assuming the material state at time t_n to be known. The goal of the solution strategy is to find the material state at time $t_{n+1} = t_n + \Delta t$ for a given total deformation ϵ_{n+1} . Over the time interval Δt the incremental work of deformation $E_n(\epsilon_n, \Delta, q)$ is defined as

$$E_n(\epsilon_n, \Delta, q) = W^m(\epsilon_m) + \frac{1}{L}\Phi(\Delta, q) + \frac{\Delta t}{L}\psi^*\left(\frac{\Delta - \Delta_n}{\Delta t}, \epsilon, \Delta\right), \quad (23)$$

where W^m is the elastic strain energy density per unit volume of the matrix, Φ is the cohesive energy density per unit surface of the faults, the term including ψ^* represent the frictional dissipation in Δt and q is an internal variable describing the state of the fault. In order to define the cohesive energy $\Phi(\Delta, q)$, according to De Bellis et al (2016, 2017) and in line with standard cohesive theories, a simple linear decreasing cohesive law has been considered, defined by two parameters: the tensile strength T_c and the critical energy release rate G_c . The tensile strength T_c plays the role of the maximum effective traction, while G_c is the area enclosed by the cohesive law. Once the critical opening displacement $\Delta_c = 2G_c/T_c$ is attained, faults completely loose cohesion and cohesive forces vanishes. In order to enforce irreversibility in the damage law, it is assumed that upon unloading faults follow a linear elastic path up to the origin. As for the friction dissipation contribution, friction is included by means of a dual dissipation potential per unit fault area ψ^* according to the classical Coulomb model:

$$\psi^* = \mu \max\{0, (\sigma' \mathbf{N}) \cdot \mathbf{N}\} |\dot{\Delta}|, \quad (24)$$

where $\mu = \tan(\phi')$ is the friction coefficient, $(\sigma' \mathbf{N}) \cdot \mathbf{N}$ is normal component of the traction vector on fault plane and $|\dot{\Delta}|$ the norm of the displacement jump rate.

The solution of the incremental problem is obtained by minimizing the incremental work of deformation accounting for the constraints provided by the impenetrability of the closed faults (i.e. $\Delta_N \geq 0$) and the irreversibility of damage (i.e. $\Delta q \geq 0$). With the inclusion of an extra energetic term, that describes the accommodation of the faults within the outermost fault or the external container through a length scale L_0 , and of an additional constraint on the norm of the orientation \mathbf{N} , the minimization process provides the unknown spacing and orientation of the faults. The model accounts for material failure both in tension (according to the Galileo-Rankine criterion) and in shear (according to the Mohr-Coulomb criterion). Further details of the model and the

mathematical expressions can be found in De Bellis et al. (2016). From the practical point of view, the model is characterized just by 6 parameters:

- The Young modulus E and the Poisson ratio ν , describing the elastic behaviour of the homogeneous matrix, i.e. the behaviour of the material in the pre-failure stage;
- The friction angle ϕ' and the tensile strength T_c , describing the failure properties of the rock according to the Mohr-Coulomb failure criterion;
- The critical energy release rate G_c ;
- A scale parameter L_0/Δ_c .

The model proved able to reproduce the triaxial response of different type of rock, both in the pre- and post-peak stages, as shown in De Bellis et al (2016, 2017) and Della Vecchia et al (2016).

In the context of the determination of the in-situ stress state, numerical simulations with the advanced model have been performed with the aim of providing a validation of the simplified analytical model presented in Step 4. The excavation of a vertical borehole within a horizontally bedded rock formation has been simulated via the Finite Element method, starting from a computational domain that includes a 1 m thick, 40 m wide horizontal square layer perpendicular to the borehole axis. The finite element mesh consists of 8,010 nodes and 36,086 tetrahedral elements. The simulation of the excavation is achieved numerically by removing (or deactivating) the elements that fall at the interior of a cylindrical cavity, whose radius takes the value $D = 1$. The model is able to predict the evolution of stress concentration around the borehole, together with the development of shear-induced, in correspondence to the maximum deviatoric stress, and tensile fractures. In the context of this paper, Figure ?? shows the elements (red spheres) characterized by the presence of shear induced fractures for two different stress anisotropy ratios S'_H/S'_h , equal to 4.0 and 4.5, for the Chelungpu example. The material parameters used are listed in Table ?. As expected, the higher the anisotropy ratio in the horizontal plane, the larger the amplitude of the failed zone. By a visual evaluation of the amplitude of the failed zone, the relationship between θ_b and S'_H can be estimated, according to the advanced constitutive model proposed. It is worth noting that, due to the stress redistribution induced by the failed elements, the numerical model has the built-in capability in accounting for the variation in borehole shape (i.e. ovalization) induce by breakout failures.

E	ν	μ	T_c	G_c	L_0/Δ_c
[kPa]	[-]	[-]	[kPa]	[kN/m]	[-]
$13.7 \cdot 10^9$	0.35	0.7	29,800	0.005	1

Table 3 Material parameters introduced in the numerical simulations for Chelungpu-B

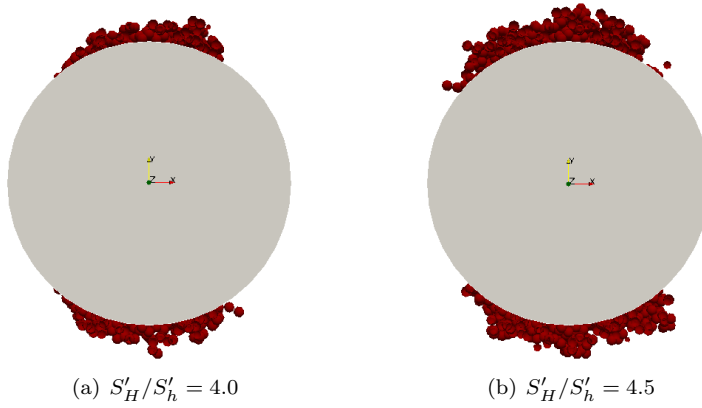


Fig. 8 Evolution of the zones subjected to shear failures at varying far-field stress anisotropies

Simulations have been carried out by varying the value of S'_H at a constant S'_h , measuring the resulting breakout amplitude, if any. Results of the simulation in terms of breakout amplitude for different S'_H values are indicated with black points in Figure ?? for the Chelungpu site, while the continuous line represents the outcome of the simplified analytical procedure (eq. ??). Despite the strong assumptions at the basis of the analytical procedure, the accordance between the two prediction is remarkably good, at least for breakout amplitudes not exceeding 90° . It is worth noting that, for parameter calibration, real data coming from the relevant literature have been used: however, available information is generally limited to friction angle and uniaxial compressive strength, which can be related to the tensile strength according to the Mohr-Coulomb failure criterion. As for the elastic parameters, E and ν , typical values for any kind of rock can be easily found in the literature. The remaining parameters are more complex to determine: in order to avoid to consider them as variables that can be used a posteriori to fit the analytical equation, sensitivity analyses have been performed in order to highlight their role for the problem at hand: as shown in Scelsi (2017), the evolution of θ_b with the far-field stress is not significantly influenced by G_c and L_0/Δ_c . Values of these parameters have just been taken from the literature (e.g. De Bellis et al. (2016, 2017), Della Vecchia et al. (2016)), without any significant influence on the numerical validation.

4 Experimental and numerical validation of case histories from the literature

In this section, a further numerical and experimental validation of the proposed simplified procedure is presented, basing on two case histories presented in the literature.

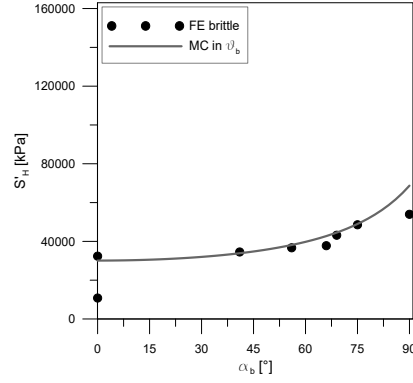


Fig. 9 Chelungpu, Hole-B (1000 m depth); comparison between the simplified analytical model and numerical results.

4.1 Basel 1 enhanced geothermal system

In 2006 a 5-km-deep borehole has been drilled under the Swiss city of Basel with the aim of developing an "Enhanced Geothermal System" EGS for a geothermal power plant. The orientation of the maximum horizontal principal stress has been determined from the observations of failures derived from ultrasonic televiewer images in 2 vertical boreholes. In the granite, tensile fractures are present in intermittent way, while breakout are present almost continually, a part from the first 100 m where they are sparse. The mean orientation of S_H from tensile and breakout failures is $N143^\circ E \pm 14^\circ$. Information about material properties and in situ stress state can be found in different studies presented in the literature (e.g. Valley & Evans, 2015, Haring et al., 2008). The profile of the breakout width is also available along the whole depth of borehole Basel-1. In the following, the stress state at 4,632 m will be analysed, where the measurement of S_h is available ($S'_h = 74.4$ MPa). Rock properties and the known effective stress state, taken from Valley & Evans (2015), are listed in Table ??.

Property	Value
S'_v [MPa]	69.6
S'_h [MPa]	28.9
ϕ' [°]	44
C [MPa]	167
θ_b [°]	≈ 60

Table 4 Data used in the study of Basel-1 at 4.632 km depth (Valley & Evans, 2015).

The analytical procedure have been applied according to the following steps:

- Step 1: limits on the stress state from the tectonic regime
The polygon of the admissible stress states in the plane $S'_H - S'_h$ is represented considering all faulting regimes. Figure ?? allows to identify graphically the first limits on S'_H : this value has to be between $S'_h = 28.96$ MPa by definition and 160.73 MPa ($S'_H/S'_h = 5.6$), i.e. limit deriving from strike-slip regime. From the polygon it can be easily deduced that the tectonic regime can be either normal or strike-slip.
- Step 2: limits on the stress state from failure orientation
Principal stresses are computed using the relation defined by Equations (??) for $\theta = 0$ and from Eq. (??) at $\theta = \pi/2$. The components corresponding to the minimum, intermediate and maximum principal stress can be seen in Figure ?? for admissible tensional anisotropies S'_H/S'_h , i.e. $1 \leq S'_H/S'_h \leq 5.6$. It can be observed that:
 - $\sigma'_r < \sigma'_z < \sigma'_\theta$ in $\theta = \pi/2$ for all the values of S'_H/S'_h , apart from anisotropies $S'_H/S'_h < 1.2$ for which the vertical stress is greater than the hoop stress. The presence of visual observations of failure directions could thus allow a further refinement of S'_H bounds;
 - in $\theta = 0$, since no tensile fractures are registered at the considered depth, the relation between stress components cannot be used to further limit the anisotropy S'_H/S'_h .

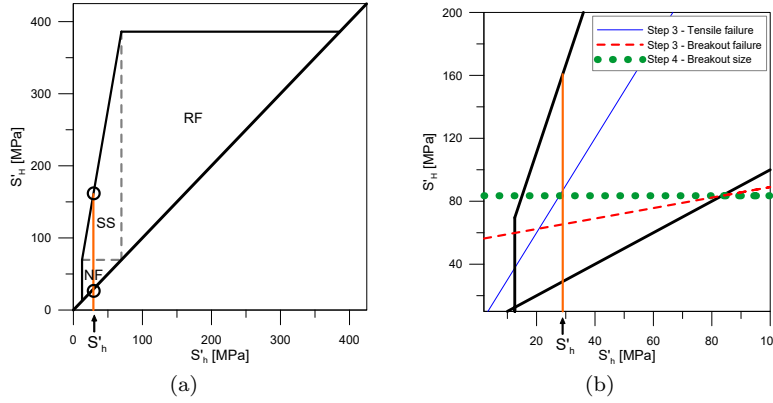


Fig. 10 (a) Admissible stress polygon. (b) Lines dividing stresses associated to different type of failures. The blue thin solid line represents tensile fractures, red dashed line the shear failures in $\theta = \pi/2$. The green dotted line indicates the value of S'_H at $\theta_b = 60^\circ$, according to Eq. ??.

- Step 3: limits on the stress state from rock failure criterion
Breakout failures have been registered in the section taken into account, while tensile fractures are absent. The Mohr-Coulomb failure criterion with tension cut-off is assumed to hold ($\phi' = 44^\circ$, $C = 167$ MPa, $S_T = 0$ MPa). The lines delimiting the presence or absence of fractures are drawn in the stress polygon (Figure ??); the stress state has to lie below the line repre-

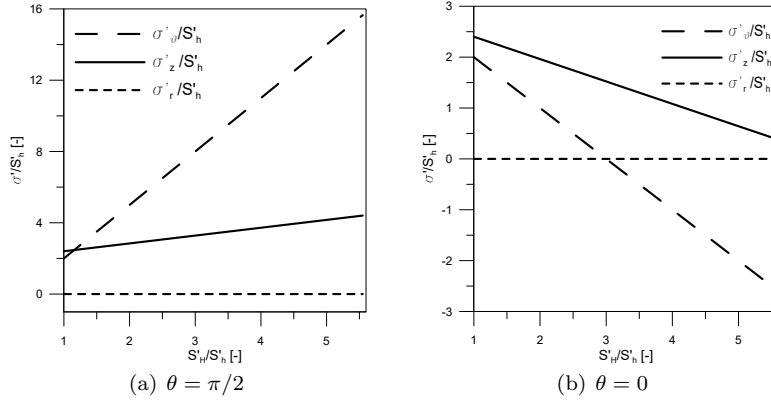


Fig. 11 Visualization of the relation between normalized principal components as a function of S'_H/S'_h , limited between admissible values derived by tectonic limits; $\nu = 0.22$, $p_{net} = 0$.

senting tensile fractures, and above the line delimiting breakout failures.

Considering the absence of tensile fractures, it can be stated that S'_H has to be smaller than 86.88 MPa; for shear failures in $\theta = \pi/2$ $S'_H > 65.32$ MPa.

Therefore $2.3 < S'_H/S'_h < 3.0$.

- Step 4: accounting for breakout size

Being the breakout angle approximately known ($\theta_b \approx 60^\circ$, corresponding to an amplitude $\alpha_b \approx 60^\circ$), a single value of the maximum horizontal *far-field* stress state can be determined. According to eq. ??, $S'_H \simeq 83.50$ MPa (corresponding to $S'_H/S'_h = 2.9$) and thus $S_H = 128.94$ MPa. This value falls between the limits obtained in Step 3.

The tectonic regime is strike-slip, as it is clearly shown in Figure ?. The maximum horizontal stress ($S_H = 128.94$ MPa) differs of about 10 MPa from the value estimated by Valley & Evans (2015) with the equation $S_H = 1.04z + 115$ MPa/km which gives a result equal to 119.82 MPa.

Step	$S'_H{}^{min}$ [MPa]	$S'_H{}^{max}$ [MPa]	Information needed
1	28.96	160.73	Broad estimate of ϕ'
2	Data not available	Data not available	Visual information of failures
3	65.32	86.88	C , ϕ' , S_T
4	83.50	83.50	C , ϕ' , breakout width

Table 5 Bounds for S'_H for each step using the proposed procedure for Basel-1 at 4632 m

Table ?? summarises the bounds for S'_H for each step of the proposed approach for the Basel-1 borehole at 4632 m.

The maximum horizontal stress obtained via the analytical procedure has been also validated by means of the numerical model described in Section ?. Ma-

terial parameters are listed in Table ??, while the principal stress components S'_v and S'_h and the breakout width have been introduced in Table ??.

E	ν	μ	T_c	G_c	L_0/Δ_c
[kPa]	[-]	[-]	[kPa]	[kN/m]	[-]
$65 \cdot 10^6$	0.22	0.97	36700	0.005	1

Table 6 Material parameters introduced in the numerical simulations for Basel-1.

Different simulations have been carried out by varying S'_H between 28960 kPa (corresponding to $S'_H/S'_h = 1$) and 159280 kPa (corresponding to $S'_H/S'_h = 5.5$), measuring for each simulation the predicted breakout width. The obtained results are plotted in Figure ??, together with the S'_H trend obtained at Step 4 via eq. ??. The numerical and analytical predictions are substantially essentially coincident up to an anisotropy ratio $S'_H/S'_h = 4$ equal to 4 and to a width $\alpha_b \approx 90^\circ$, the maximum relative error being lower than 15%.

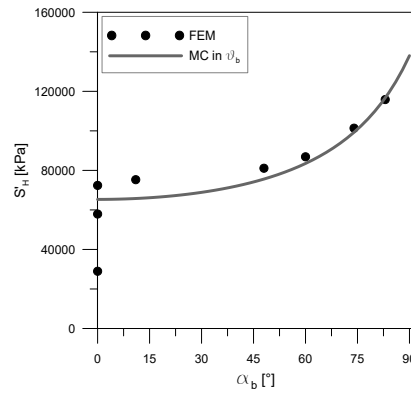


Fig. 12 Basel-1; evaluation of S'_H through the Mohr-Coulomb failure criterion imposition in $\theta = \theta_b$ and results of simulations with brittle damage model.

4.2 Cajon Pass Scientific Research Borehole

At the Cajon Pass site (California) a scientific research borehole was conducted between 1986 and 1987, reaching a depth of 3500 m. In the literature several publications (Zoback & Healy (1992), Vernik & Nur (1992), Vernik & Zoback (1992)) provide information regarding the material characteristics and the in situ stress state; some minimum horizontal principal stress S_h measurements and the amplitude of the breakout for depths between 907 m and 3486 m have

been obtained respectively via hydraulic fracturing and borehole televiewer. In this case a depth of 2048 m has been considered, where an estimate of the maximum horizontal stress S_H is available in Zoback & Healy (1992). Rock properties and the known stress state are listed in Table ??.

Property	Value
S'_v [MPa]	32.15
S'_h [MPa]	19.81
ϕ' [°]	39
C [MPa]	132
T_0 [MPa]	13
θ_b [°]	≈ 73

Table 7 Data used in the study of Cajon Pass at 2.048 km depth.

The analytical procedure have been applied according to the following steps:

- Step 1: limits on the stress state from the tectonic regime
The polygon of the admissible stress states in the plane $S'_H - S'_h$ is represented considering all faulting regimes. Figure ?? allows the graphical identification of the first limits on S'_H : this value has to be between $S'_h = 19.81$ MPa by definition and 85.75 MPa ($S'_H/S'_h = 4.3$), i.e. limit deriving from strike-slip regime. From the polygon it can be deduced that the tectonic regime can be either normal or strike-slip.
- Step 2: limits on the stress state from failure orientation
Principal stresses are computed using the relation defined by Equations (??) for $\theta = 0$ and from Eq. (??) at $\theta = \pi/2$. The components corresponding to the minimum, intermediate and maximum principal stress can be seen in Figure ?? for admissible tensional anisotropies S'_H/S'_h , i.e. $1 \leq S'_H/S'_h \leq 4.3$. It can be observed that:
 - $\sigma'_r < \sigma'_z < \sigma'_\theta$ in $\theta = \pi/2$ for all the values of S'_H/S'_h . The presence of visual observations of failure directions could thus allow a further refinement of S'_H bounds.
 - in $\theta = 0$, since no tensile fractures are registered at the considered depth, the relation between stress components cannot be used to further limit the anisotropy S'_H/S'_h .
- Step 3: limits on the stress state from rock failure criterion
Breakout failures have been registered in the section taken into account, while tensile fractures are absent. The Mohr-Coulomb failure criterion with tension cut-off is assumed to hold ($\phi' = 39^\circ$, $C = 132$ MPa, $S_T = 0$ MPa). The lines delimiting the presence or absence of fractures are inserted in the stress polygon (Figure ??); the stress state has to lie below the line representing tensile fractures, and above the line delimiting breakout failures.

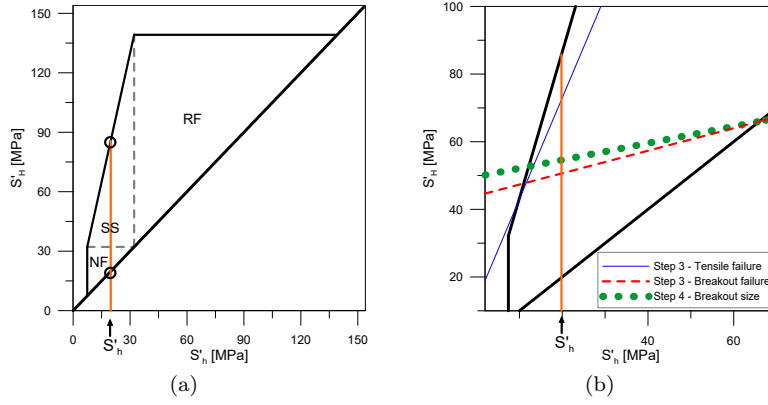


Fig. 13 (a) Admissible stress polygon. (b) Lines dividing stresses associated to different type of failures. The blue thin solid line represents tensile fractures, red dashed line the shear failures in $\theta = \pi/2$. The green dotted line indicates the value of S'_H at $\theta_b = 73^\circ$, according to Eq. ??.

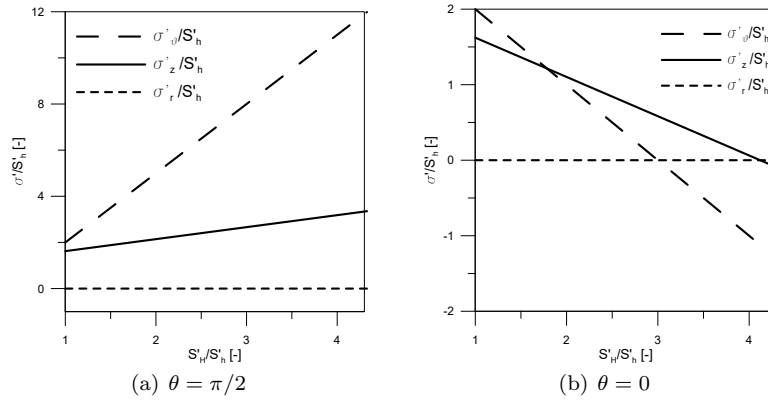


Fig. 14 Visualization of the relation between normalized principal components as a function of S'_H/S'_h , limited between admissible values derived by tectonic limits; $\nu = 0.26$, $p_{net} = 0$.

Considering the absence of tensile fractures, it can be stated that S'_H has to be smaller than 72.43 MPa; for shear failures in $\theta = \pi/2$ $S'_H > 50.60$ MPa. Therefore $2.6 < S'_H/S'_h < 3.7$.

- Step 4: accounting for breakout size

Being the breakout angle approximately known ($\theta_b \approx 73^\circ$, corresponding to an amplitude $\alpha_b \approx 34^\circ$), a single value of the maximum horizontal *far-field* stress state can be determined. According to eq. ??, $S'_H \simeq 54.56$ MPa (corresponding to $S'_H/S'_h = 2.8$) and thus $S_H = 74.7$ MPa. This value falls between the limits obtained in Step 3.

The tectonic regime is strike-slip, as it is clearly shown in Figure ?. The maximum horizontal stress ($S_H = 74.7$ MPa) differs of only 4.6 MPa from

the value estimated from hydraulic fracturing data, equal to 79.3 MPa, reported in Zoback & Healy (1992).

Table ?? summarises the bounds for S'_H for each step of the proposed approach for the Cajon Pass Borehole at 2048 m.

Step	$S'_H{}^{min}$ [MPa]	$S'_H{}^{max}$ [MPa]	Information needed
1	19.81	85.75	Broad estimate of ϕ'
2	Data not available	Data not available	Visual information of failures
3	50.60	72.43	C, ϕ', S_T
4	54.56	54.56	C, ϕ' , breakout width

Table 8 Bounds for S'_H for each step using the proposed procedure for Cajon Pass Borehole at 2048 m

Material parameters are listed in Table ??, while the principal stress components S'_v and S'_h and the breakout width have been introduced in Table ??.

E	ν	μ	T_c	G_c	L_0/Δ_c
[kPa]	[-]	[-]	[kPa]	[kN/m]	[-]
$90 \cdot 10^6$	0.26	0.8	39700	0.005	1

Table 9 Material parameters introduced in the numerical simulations for Cajon Pass Borehole at 2048 m depth.

Different simulations have been carried out by varying S'_H between 19809 kPa (corresponding to $S'_H/S'_h = 1$) and 108950 kPa (corresponding to $S'_H/S'_h = 5.5$), measuring for each simulation the predicted breakout width. The obtained results are plotted in Figure ??, where a comparison with the S'_H trend, obtained via eq. ??, is shown.

Also in this case the numerical and analytical predictions are essentially coincident up to an anisotropy equal to 4 and to a width $\alpha_b \approx 90^\circ$, , being the maximum relative error lower than 3.5%.

5 Conclusion

Determination of in situ stress state is a preliminary activity necessary for any application in the field of civil and reservoir engineering, as well as for geological and geophysical applications. Among the different techniques proposed in the literature to estimate in situ stress state in rock masses, borehole methods are certainly the most diffused. For these methods to be reliable, a sound

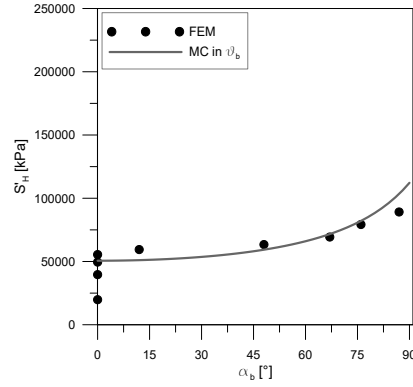


Fig. 15 Cajon Pass; evaluation of S'_H through the Mohr-Coulomb failure criterion imposition in $\theta = \theta_b$ and results of simulations with brittle damage model.

geomechanical model is needed, in order to address all the relevant characteristics of rock mechanical response that influence the behaviour of the material at the borehole scale. Unfortunately, refined models always requires a significant number of parameters, which can hardly be known without a dedicated, time consuming and expensive laboratory activity. In order to overcome such limitations, this paper presented an analytical procedure to estimate in situ stress state trying to combine a rigorous approach to the applicability of the procedure in engineering practice. In particular, the procedure is intended to be applied following some clear steps, each one requiring some input parameters and proving some bounds to the maximum horizontal stress, i.e. the most difficult stress component to determine. Step 1 stems from the application of the well-known Anderson faulting theory together with the Mohr-Coulomb failure criterion to provide some initial bounds to the stress state, exploiting information known at the reservoir scale, as already proposed in the literature. A refinement on in situ stress bounds is provided by Step 2, that just relies on visual information on failures at the borehole scale. In Authors' knowledge, this approach has never been proposed in the literature, and provides a significant reduction in stress bounds without the need of knowing rock failure parameters. Further refinement is provided by Step 3, which combine the information of the possible presence of failures at the borehole scale with the information on the failure criterion of the rock. Finally, if also breakout failure amplitude is available, a unique value of the maximum horizontal stress can be estimated via Step 4. Remarkably, just three parameters to describe rock strength have been introduced: the friction angle, the uniaxial strength and the tensile resistance. As a further advantage of the procedure, no programming or use of dedicated software is need: once the input data are known, just explicit algebraic equations are proposed.

The procedure has been then validated by means of both numerical analyses and some field data coming from the literature. Numerical analyses have been performed to check if the simplifications introduced in Step 4, involv-

ing both the mechanical behaviour of the rock and the geometry of the failed borehole, are relevant. To this aim, numerical Finite Element analyses at the borehole scale have been performed, assuming a brittle damage behaviour of the rock. The outcomes of the numerical simulations have been compared with the equations proposed in Step 4 in terms of borehole breakout dependence on stress anisotropy: the agreement between the two approaches is very good, at least for breakout amplitude lower than 90° , confirming that the assumption on which Step 4 relies are acceptable for the problem at hand. Finally, reasonable agreement has been obtained also between the predictions of the procedure with some data already present in the literature, where in situ stress estimate was performed by means of the combination of different techniques.

References

1. Aadnoy, B. S., In-situ stress directions from borehole fracture traces, *Journal of Petroleum Science and Engineering*, 4, 143-153 (1990)
2. Amadei B. and Stephansson O., *Rock Stress and Its Measurements*, Chapman & Hall, London (1997)
3. Barton C. A., Castillo D. A., Moos D., Peska P. and Zoback M., Characterising the full stress tensor based on observations of drilling-induced wellbore failures in vertical and inclined boreholes leading to improved wellbore stability and permeability prediction, *APPEA Journal*, 38, 466-487 (1998)
4. Barton C.A., Zoback M.D., Burns K.L., In-situ stress orientation and magnitude at the Fenton geothermal site, New Mexico, determined from wellbore breakouts, *Geophysical Research Letters*, 1988
5. Bell J., Practical methods for estimating in situ stress for borehole stability applications in sedimentary basins, *Journal of Petroleum Science and Engineering*, 38, 111-119 (2003)
6. Bell J.S., Gough D.I., Northeast-southwest compressive stress in Alberta: evidence from oil wells, *Earth and Planetary Science Letters*, 45 (2) 475-482 (1979)
7. De Bellis M.L., Della Vecchia G., Ortiz M., Pandolfi A., A linearized porous brittle damage material model with distributed frictional-cohesive faults, *Engineering Geology*, 215, 10-24 (2016)
8. De Bellis M.L., Della Vecchia G., Ortiz M., Pandolfi A., A multiscale model of distributed fracture and permeability in solids in all-round compression, *Journal of the Mechanics and Physics of Solids*, 104, 12-31, ISSN 0022-5096 (2017)
9. Della Vecchia G., De Bellis M.L., Pandolfi A., A multiscale microstructural model of damage and permeability in fractured solids. *Procedia Engineering* 158, 21-26 (2016)
10. Della Vecchia G., Pandolfi A., Musso G., Capasso G., An analytical expression for the determination of in situ stress state from borehole data accounting for breakout size, *International Journal of Rock Mechanics & Mining Sciences* (2014)
11. Haimson B., Lin W., Oku H., Hung J.H., Song S.R., Integrating borehole-breakout dimensions, strength criteria, and leak-off test results, to constrain the state of stress across the Chelungpu Fault, Taiwan, *Tectonophysics*, 482, 65-72 (2009)
12. Haimson B. and Rudnicki J.W., The effect of the intermediate principal stress on fault formation and fault angle in siltstone, *Journal of Structural Geology*, 32, 1701-1711 (2009)
13. Häring M. O., Schanz U., Ladner F., Dyer B. C., Characterisation of the Basel 1 enhanced geothermal system, *Geothermics*, 37, 469-495. (2008)
14. Hung J. H., Ma K. F., Wang C. Y., Ito H., Lin W., Yeh E. C., Subsurface structure, physical properties, fault-zone characteristics and stress state in scientific drill holes of Taiwan Chelungpu Fault Drilling Project, *Tectonophysics*, 466, 307-321. (2007)
15. Jaeger J., Cook N. and Zimmermann R., *Fundamental of Rock Mechanics*, Blackwell Publishing, Oxford (2007)
16. Jaky J., The coefficient of earth pressure at rest, *Journal of Society of Hungarian Architects and Engineers*, 78 (22) 355-358, (1944)

17. Leeman E., The measurement of stress in rock, Parts I, II and III. *Journal of the Southern African Institute of Mining and Metallurgy*, 65:45-114, 254-284. (1964)
18. Lin W., Yeh E. C., Hung J. H., Haimson B., Hirono T., Localized rotation of principal stress around faults and fractures determined from borehole breakouts in hole B of the Taiwan Chelungpu-Fault Drilling Project (TCDP), *Tectonophysics*, 482, 82-91 (2009)
19. Moos D. and Zoback M.D., Utilization of observations of well bore failure to constrain the orientation and magnitude of crustal stresses: application to continental deep sea drilling project and ocean drilling program boreholes, *Journal of Geophysical Research*, 95, 9305-25 (1990).
20. Onaisi A., Sarda J.P. and Bouteica M., Experimental and theoretical investigation of borehole breakouts, in *Proc. 31st US Symp. Rock Mech.*, Golden, Balkema, Rotterdam, 703-710 (1990).
21. Scelsi G., Determinazione dello stato di sforzo in situ a partire da dati di scavo di pozzo, MSc Thesis, Politecnico di Milano (2017) ?????
22. Schmidt B., Discussion paper. Earth pressure at rest related to stress history, *Canadian Geotechnical Journal*, 3 (4) 239-242, (1966).
23. Valley B., Evans K.F., Estimation of the Stress Magnitudes in Basel Enhanced Geothermal System. *Proceedings World Geothermal Congress*, Melbourne, Australia, 19-25 April 2015. (2015)
24. Vernik L. and Nur A., Petrophysical Analysis of the Cajon Pass Scientific Well: Implications for Fluid Flow and Seismic Studies in the Continental Crust, *Journal of Geophysical Research*, 97, B4, 5121-5134 (1992)
25. Vernik L. and Zoback M. D., Estimation of maximum horizontal principal stress magnitude from stress-induced well bore breakouts in the Cajon Pass Scientific Research borehole, *Journal of Geophysical Research*, 97, B4, 5109-5119 (1992).
26. Wang J.H., Thermal and pore fluid pressure history on the Chelungpu fault at a depth of 1111 m during the 1999 Chi-Chi, Taiwan, earthquake, *Journal of Geophysical Research*, 116, B03302 (2011) ???
27. Weibols G.A. and N.G.W. Cook, An energy criterion for the strength of rock in polyaxial compression, *International Journal of Rock Mechanics & Mining Sciences*, 5, 529-549, (1968).
28. Wiprut D., Zoback M., Constraining the stress tensor in the Visund Field, Norwegian North Sea: Application to wellbore stability and sand production. *International Journal of Rock Mechanics & Mining Sciences*, 37, 317-336. (1999) o 2000
29. Wu H. Y., Ma K. F., Zoback M., Boness N., Ito H., Hung J. H. and Hickman S., Stress orientations of Taiwan Chelungpu-Fault Drilling Project (TCDP) hole-A as observed from geophysical logs, *Geophysical Research Letters*, 34 (2007)
30. Zang A., Stephansson O., *Stress Field of the Earth's Crust*, London, Springer (2010)
31. Zheng Z., Kemeny J. and Cook N.G.W., Analysis of borehole breakouts, *J. geophys. Res.*, 94, 7171-7182 (1989).
32. Zoback M., *Reservoir Geomechanics*, Cambridge University Press, Cambridge (2007)
33. Zoback M.D, Barton C.A., Brudy M., Castillo D.A., Finkbeiner T., Grollimund B.R., Moos D.B., Peska P., Ward C.D., Wiprut D.J., Determination of stress orientation and magnitude in deep wells, *International Journal of Rock Mechanics and Mining Sciences*, 40, 1049-1076 (2003)
34. Zoback M. D., Healy J. H., In Situ Stress Measurements to 3.5 km Depth in the Cajon Pass Scientific Research Borehole Implications for the Mechanics of Crustal Faulting. *Journal of Geophysical Research*, 97, 5039-5057. (1992)
35. Zoback M. D., Mastin L. and Barton C., In-situ Stress Measurements In Deep Boreholes Using Hydraulic Fracturing, Wellbore Breakouts, And Stonely Wave Polarization, in *Proc. ISRM International Symposium*, International Society for Rock Mechanics (1986).
36. Zoback M. D., Moos D., Mastin L. and Anderson R. N., Well-bore breakouts and in situ stress, *J. geophys. Res.*, 90, 5523-5530 (1985).
37. Aadnøy et al (2013) ??????????????????
38. Amadei and Stephansson (1970), ??????????????????????.